Journal of Environmental Chemical Engineering 8 (2020) 104370

Contents lists available at ScienceDirect

Journal of Environmental Chemical Engineering

journal homepage: www.elsevier.com/locate/jece

Exfoliated graphite preparation based on an eco-friendly mechanochemical route

J.M. Mendoza-Duarte[a], F.C. Robles-Hernández[b], C.D. Gomez-Esparza[c], J.G. Miranda-Hernández[d], C.G. Garay-Reyes[a], I. Estrada-Guel[a,*], R. Martínez-Sánchez[a]

[a] Centro de Investigación en Materiales Avanzados (CIMAV). Laboratorio Nacional de Nanotecnología, Miguel de Cervantes No. 120, 31136, Chih, Mexico
[b] Department of Mechanical Engineering Technology, University of Houston, Houston, TX77204-4020, USA
[c] Instituto de Ingeniería y Tecnología, Universidad Autónoma de Ciudad Juárez (UACJ), Av. Del Charro 450 norte, Cd. Juárez, 32310, Chih, Mexico
[d] Universidad Autónoma del Estado de Mexico, Centro Universitario UAEM Valle de Mexico, 54500Atizapán de Zaragoza, Edo. Mexico, Mexico

ARTICLE INFO

Keywords:
mechanochemical
graphite exfoliation
high-energy ball milling
green method
MB adsorption
wastewater

ABSTRACT

In the present study, we proposed an eco-friendly method to produce exfoliated graphite based on a dry mechanochemical process. This route represents an alternative that avoids the use and disposal problems related to highly corrosive and dangerous reagents use, manipulation and elimination. As non-toxic alternative exfoliation route, an equimolar mixture of graphite flakes and calcium carbonate was milled and leached with an aqueous solution of acetic acid (vinegar). There was a notable reduction of the graphite particle size with a significantly increased level of exfoliation, which dramatically improved the surface area of the prepared samples from 4 to 363 $m^2 g^{-1}$. After 16 h of processing, milled particles reached a *thickness reduction of up to 5* nm *and micrometric widths.*The overall yield of processed graphite is around 92% based on the raw graphite. The evident benefits of the obtained exfoliated graphites in the adsorption of methylene blue (a common pollutant of textile wastewater) are presented. Exfoliated graphite represents a valid alternative as adsorption agent for dye removal reaching efficiencies above 95% after 30 min of testing with an aqueous solution of methylene blue. Contrary, the untreated graphite sample showed a null adsorption activity.

1. Introduction

Intense, brilliant and durable colors are the key for the sales success of a large number of items produced by industries like the textile, paper, food, pharmaceuticals, cosmetics, plastics, cloth dyeing, leather, and printing: those factories consume a massive amount of dyes generating large volumes of wastewater. In emerging countries, the majority of this water is returned to nature as an untreated toxic mixture composed of hazardous chemicals and residual dyes; here, dye contaminated wastewater represents a sad visual proof of the pollution generated from these human activities. Some synthetic dyes can be deposited in living beings with adverse accumulative effects in the food chain [1]. Green alternatives are the natural dyes for textile coloration, but they are not employed on an industrial scale due to their higher cost and limited availability. Synthetic dyes usually have complex aromatic molecular structures that enhance their stability against heat and light, making them challenging to biodegrade; their disposal in water bodies often exhibits severe adverse effects on the environment. Azo dyes are the primary synthetic type of chromogenic released materials; they are characterized by one or more azo groups (N = N) as chromophores, with aromatic containing groups. Unfortunately, they are a popular option for textile coloration because they can be used at lower temperatures and release rich color depths, although some are listed as possible carcinogens. Methylene blue (MB) is a primary basic azo dye used for coloring purposes and a common pollutant material in textile wastewater [2]. From a diverse group of available techniques for dye removal from wastewater, the solid surface adsorption is getting increasing attraction in the field due to its low-cost, simplicity, ease of operation [3]–[5] and “the activation of the components” can increase the removal capacity of dyes, pigments and other organic pollutants significantly [6].

Although carbon is known since ancient times, it was not until the last decade that a two-dimensional array of atoms bonded together in a honeycomb lattice called graphene appears in literature [7]. This material rapidly got attention due to its extraordinary electrical, thermal, and optical properties [8,9]. However, practical applications have not been as promising as was initially envisaged due to associated fabrication issues [10]. Today, the scalable production of graphene remains a considerable challenge [11]. There are some routes to produce graphene with high crystal quality, but they are impractical for

* Corresponding author.

https://doi.org/10.1016/j.jece.2020.104370
Received 25 February 2020; Received in revised form 6 August 2020; Accepted 9 August 2020
Available online 14 August 2020

commercial applications due to low production rates and high-related costs [12]. Expanded or exfoliated graphite (EG) has a good chemical affinity for organic compounds and polymers based on its structure formed for multiple carbon layers. This particular array is weakly ionic and hydrophilic; consequently, the superficial adhesion for organic molecules is improved (in the form of a high wettability) due to the presence of external electrostatic forces. Therefore, EG can be used as a multi-compositional filler [13], thermal isolation component [14], adsorbent for oil spilled in water [15]–[17] and material for organic dyes removal [2,3,5, 6]. There is a wide variety of preparation methods for EG, where the chemical route has received intense interest because of its scalability and low production costs [12]. EG, is obtained by rapid heating of graphite (Gr) intercalation compounds with Brønsted acids [18] based on the original and modified Hummers method [19]. In this method, Gr is treated with mixtures of strong acids and oxidizing agents such as concentrated sulfuric-nitric mixtures [13], perchloric acid [20], sodium permanganate [15], highly-concentrated hydrogen peroxide [8,21] to expand the interplanar spacing of Gr for chemical intercalation. An alternative route that avoids the use of aggressive acids and oxidants has been described, based on a heterogeneous gas-solid reaction [22], forming fluorinated graphene. However, the processing is a real challenge because of the high reactivity of pure fluorine gas even when it is diluted with an inert gas [23]. Another vigorous oxidizer and fluorinator used is chlorine trifluoride. There is a safer and scalable mechanochemical synthesis of fluorinated graphenes avoiding the use of fluorine [24], but calcium hypochlorite is necessarily used for chlorination. However, this chemical is clearly more corrosive compared to the calcium carbonateused in this work. Other methods avoid the use of strong acids using sonication [19], solvents, exfoliation by high temperature [22] or electrochemical techniques [21]. Each method contains significant problems, like the use of expensive equipment, complicated chemical processing, and low yield of production. Liquid-phase exfoliation is an efficient way to obtain graphene by sonication of the bulk material in organic solvents [25]. Moreover, during Gr exfoliation in aqueous solutions (organic solvent-free), the addition of surfactants is necessary to stabilize graphene suspensions. However, surfactants are often quite tricky to eliminate, thus exerting adverse effects on the properties that make graphene unique [11]. On the other hand, the electrochemical exfoliation route is a cost-effective and green approach in graphene synthesis [26]. Unfortunately, its low production rate level of a few grams per day limited to its practical use [27]. Mechanical ball-milling is a powerful and versatile technique to produce particles of controlled-size with a homogeneous composition. For EG preparation, ball milling and some additives were used as exfoliant agents [28]. Some works used this principle, but there are negative points to be considered: Posudievsky et al. used NaCl as a dispersant for solvent-free mechanochemical delamination of Gr, but only 50 mg of Gr were processed per batch and required expensive and time-consuming sonication-centrifugation additional processing [29]. Other work prepared by milling a few milligrams of Gr with organic nitrogenated compounds that are cataloged as toxic for fish and other aquatic invertebrates [30]. Liquid phase exfoliation with wet ball milling at low temperatures requires the use of solvents that are toxic for the environment [31]. Carboxylation via mechanochemical processing used dry ice (CO_2), extended milling periods (48 h), and acid solutions for extraction to remove metallic impurities [32].

Looking for an eco-friendly, simple and cheap alternative to produce EG for possible applications, we present an alternative method that consists of the solid phase exfoliation of Gr using a mechanochemical procedure and a leaching step which avoids the use of corrosive and dangerous chemicals. In this study, calcium carbonate ($CaCO_3$) was chosen as a green exfoliating agent because of its high availability, low cost, high abrasive nature, and easy removal with weak carboxylic acids. Moreover, it is a cheap compound commonly found on earth, living organism's components, and is particularly non-toxic. To remove this compound (after milling), acetic acid was used; it is classified as weak and not toxic, commonly found in grocery stores and our kitchens. Diluted with water (3-9% by volume) is colloquially known as vinegar and has been used as a medicine/antiseptic for thousands of years. The reaction remnants are composed of an aqueous solution of free acetic acid and calcium acetate. Both chemicals are non-toxic and well known for their frequent use as a food additive, stabilizer, buffer, and chelating agent in the food industry. Another practical advantage of calcium acetate is its high recyclability; it can be crystallized and heated, producing fresh exfoliating and washing acid following the chemical reaction between 340 and 480 °C:

$$Ca(CH_3CO.O)_2 \rightarrow CaCO_3 + CH_3CO.OH$$

Two exfoliated graphite samples prepared following our alternative green method and the original graphite (used as reference) were tested as potential adsorbent agents for removing a dye from a prepared solution simulating wastewater. MB dye was chosen because this cationic heterocyclic aromatic thiazine is frequently selected as a model organic compound to evaluate the behavior of sorbent for the removal of organic pollutants from its aqueous solutions [2].

2. Experimental details

2.1. Materials

Natural Gr (flakes, -10 mesh, 99.9% purity from Alfa Aesar Co.) was used as raw material. Meanwhile, Calcium carbonate (99.5%), acetic acid glacial (99.9%), and deionized water from JT Baker (analytical grade) were used as exfoliating agents. The mechanochemical exfoliation of Gr was performed following a two steps procedure:

3. Samples preparation

3.1. Solid-phase exfoliation

An Equimolar mixture of Gr-$CaCO_3$ was prepared and processed in a SPEX 8000 M high-energy mill equipped with a 55 mL capacity hardened D2-steel container, and six steel-chromium coated balls (3 × 13 and 3 × 11 mm) were used as milling media. Approximately 8 g of $CaCO_3$-Gr mixture was processed utilizing a ball to sample ratio of 5:1 (in weight). The milling intensity was set to 0, 1, 2, 4, 8, and 16 h under an air atmosphere. A 0 h sample (used as reference), was obtained introducing the mixture in the container without balls and was stirred for 3 min in the mill for homogenization.

3.2. Leaching process

The milled mixture was stirred in a flask with 500 mL of an acetic acid aqueous solution (8% vol./vol.) and mixed at 300 rpm using a Corning PC420D magnetic stirrer for 2 h. The resulted suspension was filtered and washed with deionized water. The paste was dried in an oven at 80 °C for 10 h. Powders were collected and manually homogenized using a mortar and pestle. GE recovery was calculated to be 91.5%. The principal loss of graphite was caused during the manipulation during milling and washing.

3.3. Characterization

The morphological and chemical studies of milled and lixiviated Gr powders were performed via scanning electron microscopy (SEM) with a JSM-7401 F field emission microscope and transmission electron microscopy (TEM) in a Hitachi 7700 microscope, both coupled with an EDS Bruker Quantax using an accelerating voltage of 100 kV. For TEM studies, powders were dispersed by sonication 2 min in ethanol and put on a carbon-coated copper grid. X-rays diffraction (XRD) was carried out using a Bruker D8 advance diffractometer, the CuKα (λ = 1.5405 Å)

generator was operated at 40 kV and 30 mA, scanning 2θ ranged from 10 to 110° with a 0.0167°/step and 5 s/step. Raman spectra were collected on a Horiba spectroscope model Lab Ram HR with a He-Ne laser (632.8 nm and ± 1 cm^{-1} in Raman shift). Surface area determination was performed by the Brunauer-Emmett-Teller (BET) equation using N_2 as adsorbate, adsorption was and performed at liquid-nitrogen temperature (77 K) and desorption at room temperature. Before BET analyses, the degassing condition consisted of the sample heating at 250 °C for 2 h under vacuum in a Quantachrome Autosorb-1 Gas Sorption System.

3.4. Adsorption batch experiments

The experimental runs were performed in a 150 mL glass beaker constantly agitated with a Corning PC-420D hot plate at room temperature. For each batch, 25 mg of the graphitic materials: original (Gr0 h), milled (Gr16hM) and milled with $CaCO_3$ and leached (Gr16hL) were suspended in 50 mL of deionized water, stirred for 3 min (at 300 rpm) and sonicated for 5 minutes in a Branson 2510 ultrasonic cleaner. After sonication, 50 mL of Methylene Blue (Sigma Aldrich M9140) solution (60 mg/L) was added with stirring. The adsorption studies were carried out up to 60 min with 10 min intervals. The suspension samples were centrifuged (2 min), and the MB concentration was determinate using a Cary 5000 UV-Vis-NIR spectrophotometer (cuvette path length, 10 mm) using deionized water as a blank. For MB determination, the standard calibration method was used by running a series of standard solutions of the dye from 0 to 30 mg/L.

The dye removal percentage was calculated according to the formula:

$$Removal\ (\%) = \frac{(Co - Ct)}{Co} X\ 100$$

And the dye adsorption capacity of the adsorbent DAC was calculated following equation:

$$DAC\ (mg/g) = \frac{(Co - Ct)}{m} V$$

Where $\mathbf{C_0}$ and **Ct** (mg/L) are the initial concentration of dye at the beginning and at time **t**, respectively; **V** is the volume of the solution (in L), and **m** is the weight of the adsorbent (in g).

4. Results and Discussion

4.1. Microstructural Characterization

The powders of the Gr-$CaCO_3$ equimolar un-milled (0 h) and milled (1 h) were cold compacted (450 MPa) and polished with fine-grit sandpaper (# 4000) to obtain more representative EDS results (this process was performed to reduce the electron beam and sample holder interactions). The micrograph in Fig. 1a shows the presence of bright zones on the sample surface, which correspond to $CaCO_3$-rich areas and the darker zones ones to carbon (Gr); it was confirmed by EDS mapping.

After 1 h of ball milling, a remarkable difference between the distributions of the constituents in the sample was noticed. Big Gr particles were not distinguishable (Fig. 1b), as shown in the elemental mappings. As can be seen in Fig. 2a and the summary tables, after the leaching process (Fig. 2b), calcium (the main element of the exfoliating agent) was eliminated, leaving carbon and oxygen as main components. This significant concentration of oxygen is derived from the treatment. Oxygen in the leached sample can be attributed to adsorption and probably a bonded structure, as will be discussed. The removed $CaCO_3$ from the powders with vinegar solution forms calcium acetate ($CaAc_2$) dissolved in the leaching and washing solutions. The resulting lixiviation solution is a harmless substance commonly used as a food additive and can be recycled to obtain precursors, as was discussed in the introduction.

In Fig. 3 it is evident that the general morphology of graphite was modified after processing due to the dominant shear stresses caused by high-energy milling. The Fig. 3a shows the initial morphology of the natural graphite where the particles exhibit the characteristic thick flake-like appearance (composed mainly of large and continuous graphite sheets). After processing, these intrinsic characteristics were modified, forming twisted graphitic nanosheets with sub micrometer lateral sizes. This behavior was described by D. A. Siddhanti et al. [24]: During milling, two acting forces are modifying the Gr morphology (Fig. 4): shear forces increase the exfoliation level meanwhile compressive forces break the Gr sheets decreasing their particle size; both effects originated by the high energy impacts of the milling media. The shear and compressive stress overcome the Van der Waals forces, maintaining the graphene layers stacked in the graphite structure. Thus Gr sheets are peeled. The final product consisted of sub micrometric sized layered structures, which are clustered in much larger particles forming big aggregates.

4.2. X-Rays Diffraction (XRD)

The Gr-$CaCO_3$ mixture (0 h) shows the high intensity and sharp peaks characteristics of crystalline materials in the diffractogram of Fig. 5a. In the milled and leached samples (1 – 16 h), the $CaCO_3$ signals are no longer perceptible, or there are below the instrumental detection level of the device. This corroborates the effectiveness of acetic acid as a leaching agent (these results were confirmed through SEM-EDS studies). Gr has three main peaks around 26.5, 44.5, and 54.4° for its planes (002), (101), and (004), respectively. An intense and sharp (002) peak observed in the 0 h sample, suggesting a highly ordered material with multiple graphene layers [7]. After processing, the (002) peak intensity of samples decreases as a function of the milling time, this is indicative of a significant reduction of the close-packed hexagonal structure, revealing the exfoliation of Gr [10] and the increase of lattice defects such as stacking disorder [33]. Moreover, there is an evident peak shifting to a lower angle, revealing that the interlayer distance among adjacent Gr sheets increases (Fig. 5b). To confirm the mentioned, the average d-spacing (002) of samples was calculated using the Bragg equation, obtaining the following values: 3.351, 3.379, 3.377, 3.390, 3.390, and 3.385 Å for 0, 1, 2, 4, 8 and 16 h samples respectively.

This change cannot be attributed to the presence of intercalation compounds with bonded-oxygen because the atomic radius of oxygen is 0.65 Å. There is no presence of new peaks attributable to other phases in the DRX patterns, as has been previously reported [34]. The broadened peaks of further processed samples indicated high disorder in the graphene restacking [9] or amorphous graphene layers presence [8]. Based on the (002) full width at half maximum (FWHM) and Scherrer equation, the average stacking height of graphene sheets was estimated [35], corresponding to 102 and 5 nm for 0 h and 16 h samples, respectively; this corresponds a significant quantity reduction of graphene from 300 to 15 layers. Fig. 5b shows a close-up around (002) peak, there is a noticeable broadening in all milled materials, indicating a rise of disorder in the [001] direction during the graphene sheets restacking [9]. Van der Waal's interaction holds the graphene sheets together, and friction forces can partially overcome these forces; this phenomenon explains the loss of long-range order due to the application of shear forces by high-energy ball milling [7].

4.3. Surface area determination

Debelak et al. mention that a positive byproduct caused by the exfoliation of Gr is the increase in surface area (SA) [13], and Tikhomirov et al. claims that the presence of amorphous carbon also induces the same effect [18]. Thus, the total SA of the samples was determined using the Brunauer-Emmett-Teller (BET) theory to measure the level of exfoliation reached following the present route. To reveal the effect of

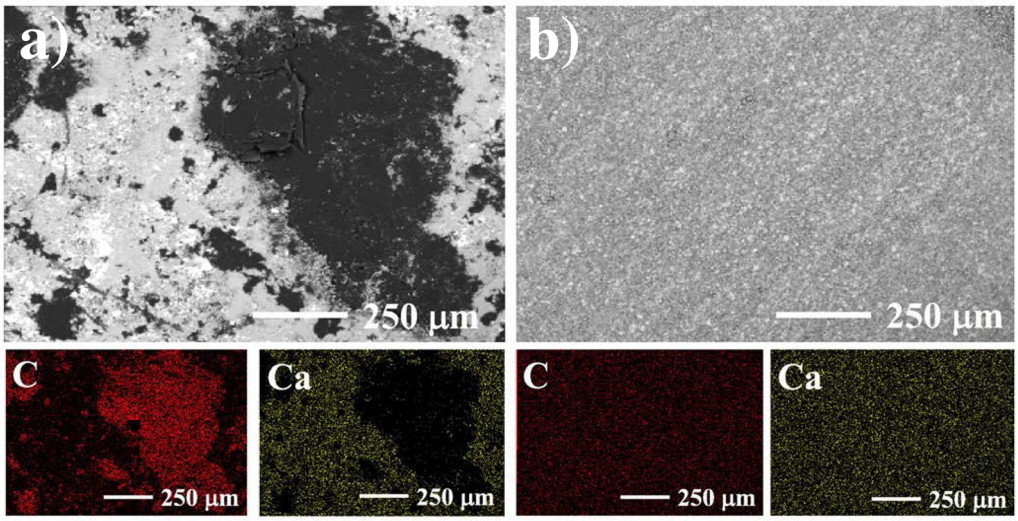

Fig. 1. SEM-BSEmicrographs of a) un-milled and b) 1 h milled samples with their respective elemental mappings.

$CaCO_3$ as an exfoliating agent, pure Gr SA results of previous works prepared using the same milling intensities and conditions are presented in this section [36,37]. The adsorption and desorption isotherms of EG samples showed a notable variation, which is dependent on the particle size and pore size distribution; both characteristics are related to the milling time. Higher intensity means more exfoliation due to the friction between milling media, graphite and $CaCO_3$, meanwhile the more significant particle size reduction because of the brittle nature of Gr, excessive shear stress and compression forces occasioned by the multiple impacts of milling media and presence of the abrasive material. As can be seen in Fig. 6, original Gr has a BET area smaller than 4 $m^2\ g^{-1}$, which was increased to 363 $m^2\ g^{-1}$ after 16 h of milling in the presence of $CaCO_3$ and the subsequent leach process. Due to the abrasive properties of the $CaCO_3$, Gr particles are easier to exfoliate than pure Gr obtaining higher values in SA (363 vs. 98 $m^2\ g^{-1}$). The shapes of the nitrogen adsorption isothermals for the processed samples from 0 to 8 h are classified into an II type according to BDDT/IUPAC classification, suggesting the existence of macropores or small particle sizes, the low hysteresis between adsorption and desorption isotherms implies a low proportion of mesopores in the samples. On the contrary, the 16 h sample presents a hysteresis loop that can be classified as a mixture of type IV (typical for mesoporous solids) and type I (for microporous materials). This SA can be considered as mainly microporous (with a peak of pore size distribution below 2 nm) and a lower contribution of mesopores. This sample presents a desorption branch related to an H3 type hysteresis loop, associated with capillary condensation in slit-shaped mesopores (2-50 nm) of plate-like particles, as was mentioned [16]. Table 1 shows some works found in the literature in the form of a comparative chart with different results related to the increase of SA in Gr following different routes.

4.4. Raman Spectroscopy

This technique has been demonstrated to be one of the most potent method to characterize graphitic structures because lattice defects in Gr disturb the hexagonal symmetry of the lattice and modify the vibrational modes observed in Raman scattering. It is also used to know the stacking order, number of layers and photon dispersion of graphene [48]. The Raman spectrum of Gr is mainly dominated by the typical D, G, and 2D bands [7]. The D band presence is an indicator of small grain sizes, defects [16], or loss of hexagonal symmetry [33].

Meanwhile, the shape, width, and position of the 2D peak are susceptible to the number of graphene layers. In single-layer graphenes, the 2D band is approximately two times stronger than the G band, decreasing with the number of layers [35]. The Fig. 7 shows Raman spectra of 0 h sample and the mechanochemical processed samples (1 to 16 h). 0 h sample has a well-resolved G band and an almost negligible D band inactive of a typical combination of graphitic carbon with large grain sizes. The presence of the 2D band is explained by the flake nature of the particles presenting a shorter order in the "c" direction of the lattice [18]. The existence of D, G, and 2D bands are typical of graphitic (sp^2) carbon, and their respective locations are 1327, 1577, and 2673 cm^{-1}. Milling promotes a high number of crystalline defects; these structural changes are related to the reduction of the G band and increase of the D band. The mentioned modification of G and D bands has been interpreted as decreased in-plane crystallite sizes on an atomic

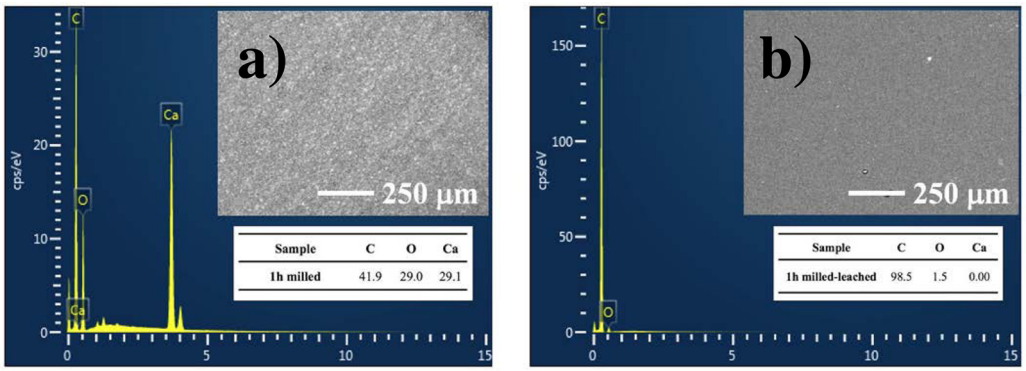

Fig. 2. EDS spectrums of 1 h sample in a) milled, b) milled-leached condition, and compositional results (in wt. %).

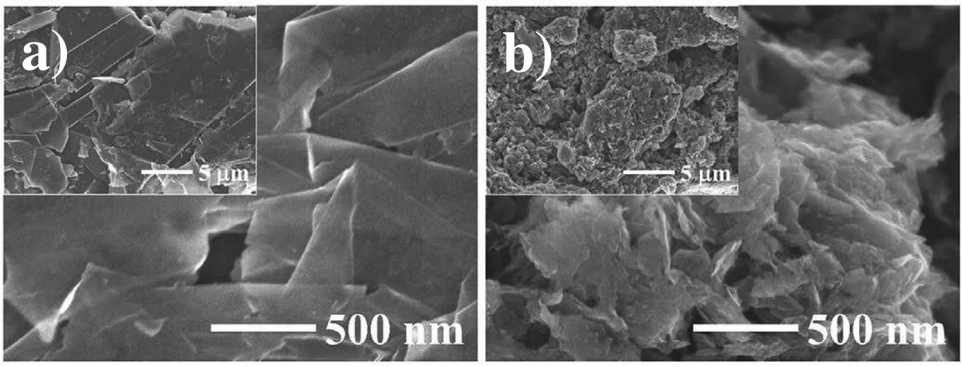

Fig. 3. SEM micrographs of a) original Gr and b) 8 h milled-leached samples.

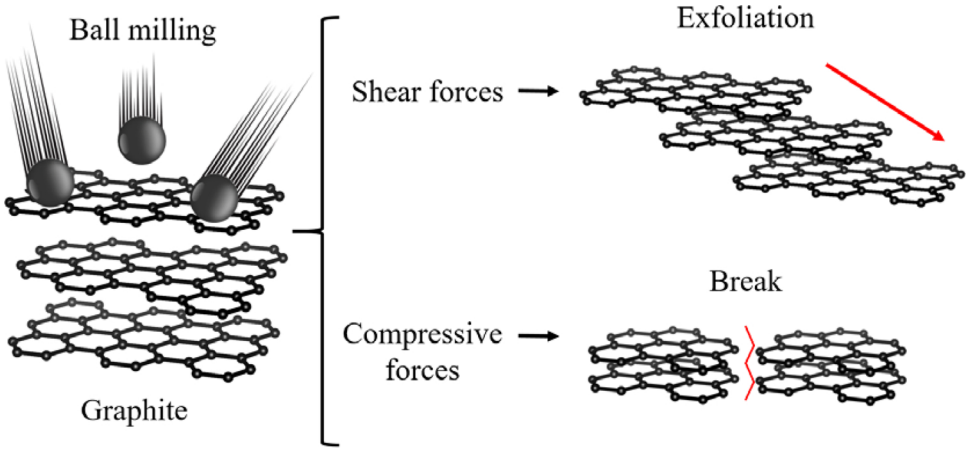

Fig. 4. Schematic representation of graphite processing by mechanical milling.

scale. This may be regarded as an increase of the graphite edges because of the smaller size of the crystallites. S. Sharma et al. mentioned, increased D-band intensities can indicate the transformation of in-plane sp^2 carbon to disordered tetrahedral sp^3 carbon domains. Meanwhile the increase in the ratio I_D/I_G, can be attributed to the rise in the disordered structure of graphite aroused from different functional groups present in the structure [49]. After milling, the intensity of D-band can exhibit the amount of the defect in graphene structures; it has been assigned to a vibrational mode that originates from the disorganized region near crystal edges, lattice defects and vacancies. Thus, low D-band intensity means relatively pristine graphitic structure. Another band which is usually related to defects, appeared at ~1620 cm^{-1} (called D1´), it appeared as a shoulder on the right side of the G band in 16 h sample. The exact nature of this Raman band is not clear. However, Wand et al. mentioned that the D1´ band arises from the vibration of C-C atoms near an interstitial carbon atom since the latter is bound to one plane and the atoms in the Gr plane are attracted towards the interstitial which may increase the C-C bonds in the plane in the vicinity of interstitial. If the force constant of the C-C bonds becomes larger, then the G band will shift towards the higher frequency side. Because of the number of interstitial carbon atoms between the aromatic planes of the carbon atoms increases with ball-milling time, the intensity of the D1´ band increases at higher milling intensities [50]. The 2D band shape is a clear indicator of the exfoliation degree and stacking order; this

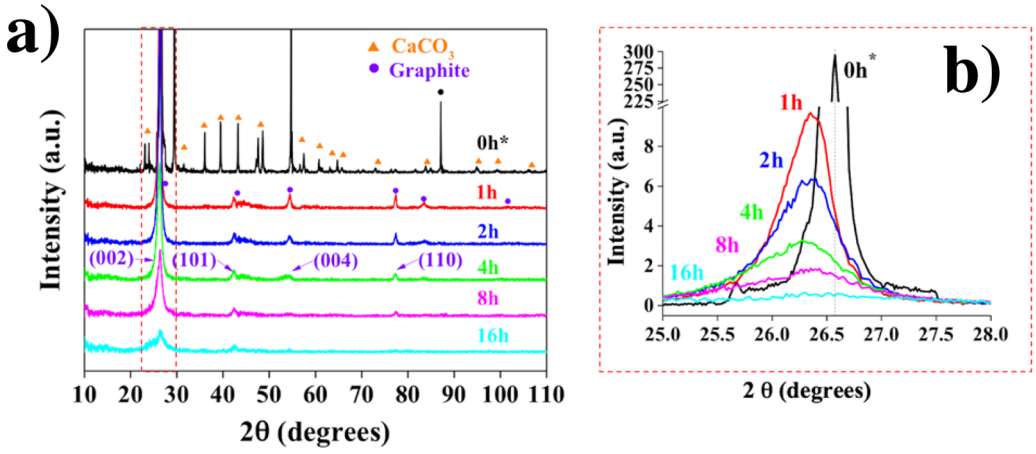

Fig. 5. XRD patterns of a) Gr-$CaCO_3$ mixture and leached samples and b) magnification of main diffraction peak.

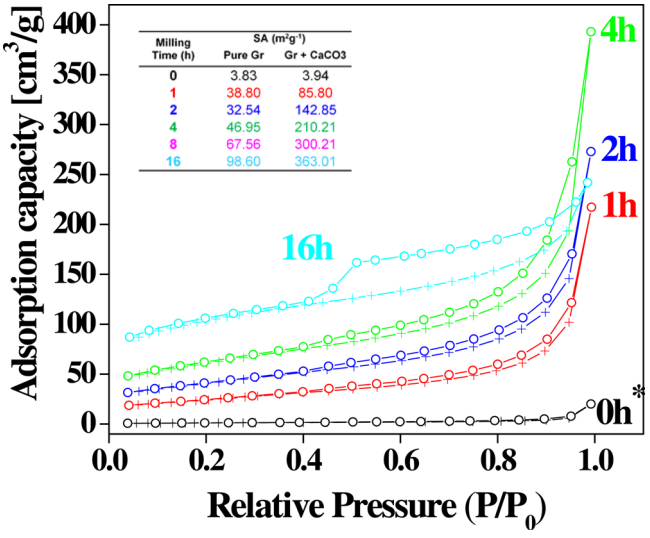

Fig. 6. Adsorption-desorption isotherms of samples and SA of pure milled Gr and leached $CaCO_3$-Gr.

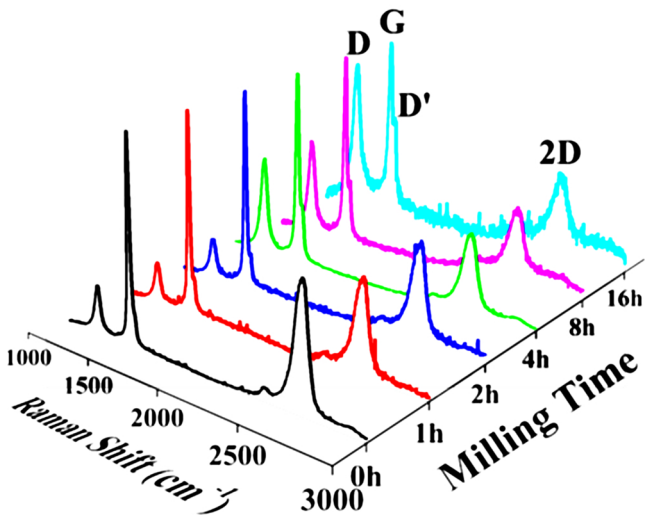

Fig. 7. Raman spectra of pure Gr (0 h) and leached samples.

band shows a shoulder around 2450 cm^{-1} in 0 h sample and early milling stages. In contrast, no shoulder was found at further milled samples (8 and 16 h); this distinction illustrates that the mechanochemical produced samples are different from crystalline Gr, and confirms the exfoliation of graphene nanosheets [11,51]. Calculating the ratio I_D/I_{D1}´, the nature of defects can be identified. The increase observed in D band as a function of milling time is also related to the distribution of the clusters with different dimensions and orders in amorphous phases. Edge-type defects were characterized by I_D/I_{D1}´ ~ 3–4.5, vacancy basal plane point defects give rise to I_D/I_{D1}´ ~ 7 and sp^3 defects to I_D/I_{D1}´ ~14 [9]. The ratio found in the 16 h sample was ~13 related to the sp^3 array. In previous publications, those arrays were identified as morphed graphenes, and their formation was related to the milling conditions [52,53].

4.5. TEM and HRTEM

Fig. 8 shows some micrographs of samples milled for 0, 1, 8, and 16 h. Graphene layers on the bright-field images were observed, it is possible to measure the d-spacing of the planes (002) [54] as is shown in the Fig. 8 obtaining values of 0.352, 0.380, 0.388, and 0.386 nm, respectively, corroborating the d-spacing values obtained by XRD. This information evidenced that high-energy ball milling increased the interlayer distance of adjacent graphene sheets in the Gr structure. Also, a decrease in particle size and an increase in density of graphene layers are observed in the function of milling time. The notable morphology changes in Gr particles are remarkable as a function of milling intensity of the generated particles. Not only the number of layers per sheet decreased, but also, the size of these layers was drastically reduced. Meanwhile, by XRD, the same samples show sizes between 31.8 and 3.8 nm. These discrepancies between Raman and XRD are because Raman predicts the length of the crystal (breath mode) while XRD is used to assess the stacking. Further, the HRTEM work confirms the presence of graphene in the processed samples with d-spacing approximately 3% different from the theoretical.

4.6. Methylene blue adsorption testing

Fig. 9a shows the absorbance spectra of the original MB solution (min 0) and samples read after the graphite addition as a function of time. Two major absorption bands characterize the absorption spectrum of MB in dilute aqueous solutions: one corresponds to a high-

Table 1
Comparative summary chart showing processing methods and some environmental disadvantages.

Synthesis method, main chemicals and related observations	SA (m^2/g)	Ref.
Gas bubble exfoliation. Gr nanosheets were obtained by melamine polymerization at 550 °C for 2 h. Toxic gases generation since melamine is obtained from formaldehyde and urea.	16.1	[38]
Chemical and thermal exfoliation. g-C_3N_4 was prepared using a few grams of bulk g-C3N4 was stirred in 8 mL concentrated H_2SO_4 for 1, 3, and 5 h.	127.63	[39]
Two kinds of GO were prepared: A) Using Brodie's method: which includes fuming nitric acid and potassium chlorate at 0 °C. Particular caution is necessary since explosions can occur. B) modified Hummers route: it includes $NaNO_3$- $KMnO_4$-H_2SO_4-$NaNO_3$-H_2O_2.	550 and 130	[40]
Graphene preparation via microwave-assisted intercalation, the waste after process (Gr, dibasic ester (DBE), Ammonia. DBE) is not considered a hazardous waste, but this process has a high consuming time.	379.2	[41]
Electrochemical exfoliation uses organic chemicals: 2-aminoanthraquinone - tert-butyl nitrite – acetonitrile and 0.1 M H_2SO_4 electrolyte.	56-64	[42]
Exfoliation and activation of graphite using microwaves the Gr + KOH solution stirred for 12 h.	60.4	[43]
Electrochemical exfoliation with high electrical energy consumption for NaCl melting and it requires Ar-4%H_2 flow.	121 and 232 at 920 °C	[10]
Graphite oxide was produced from a cyclic voltammetry method using $HClO_4$.	677.8	[44]
Hydrolysis and thermal treatments to produce expandable graphite require graphite bisulfate obtained from concentrated H_2SO_4 and high temperature.	77.3 at 1300 °C	[45]
EG was produced from Gr and intercalation of H_2SO_4.	49.7	[46]
Thermal expansion of sulfuric and nitric acid intercalated graphite, followed by the ultrasonic treatment. Acid-graphite was prepared by HNO3 and H2SO4 for 18 h.	6.94-90	[47]
Thermal decomposition of various intercalated compounds of fluorinated. Gr + liquid ClF_3 (this is an extremely reactive chemical).	141-370	[16]
Mechanochemical method uses a common chemical with very low toxicity.	38.8-363	This work

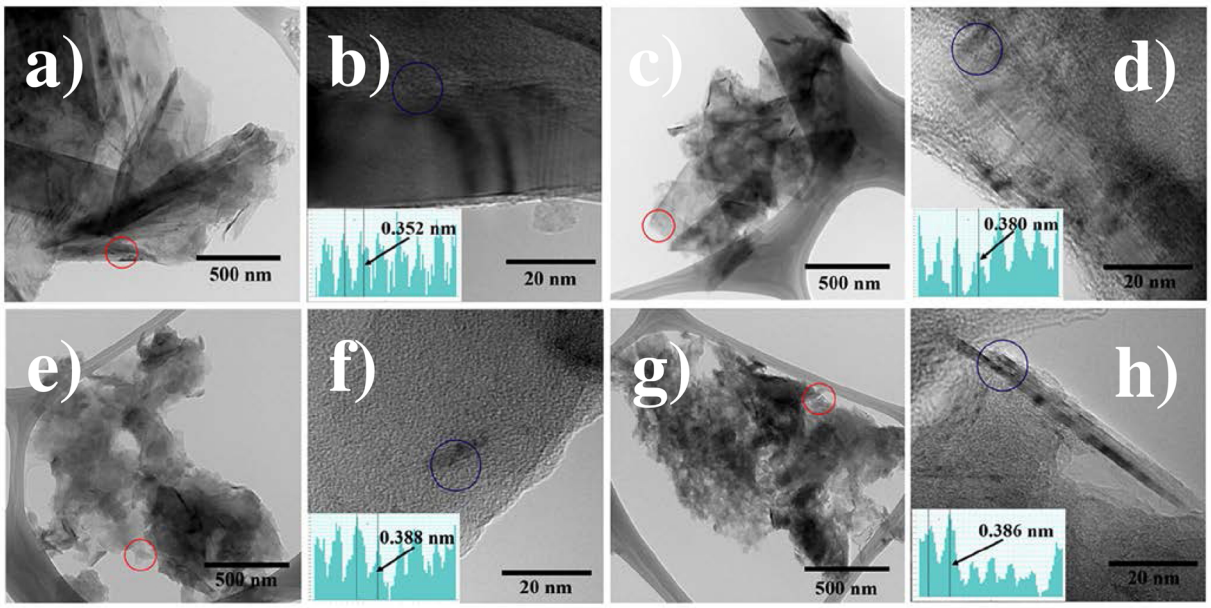

Fig. 8. BF-TEM images of samples processed during (a, b) 0 h, (c, d) 1 h, (e, f) 8 h, and (g, h) 16 h.

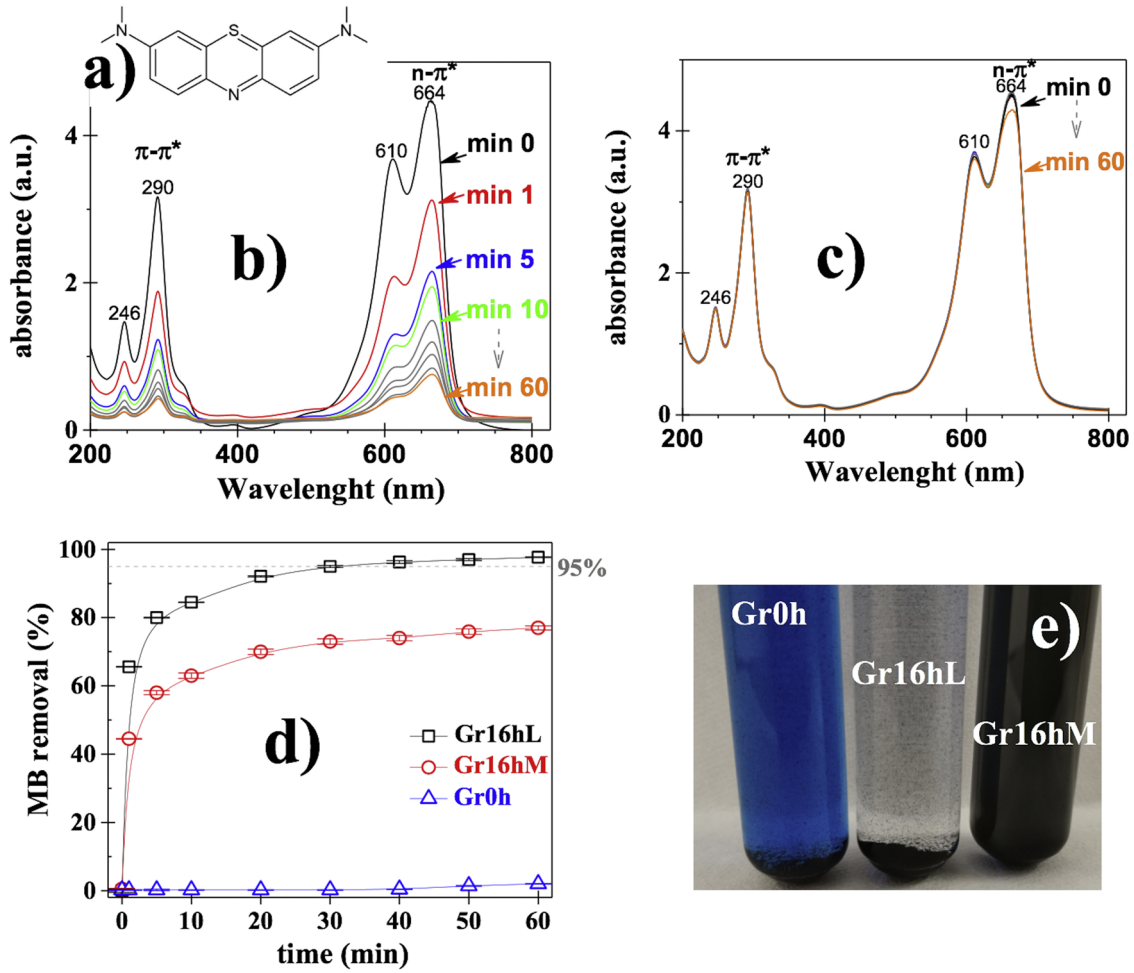

Fig. 9. (a) MB molecule, UV-vis absorption spectrum of the MB solutions read in 10 min intervals after the graphite addition: (b) Gr16hL, (c) original Gr0 h samples, (d) adsorption efficiency of samples as a function of time and (e) photograph of the suspensions after the reaction.

energy transition (π-π*) of the benzene ring which is located at 290 nm and the other of low energy found around 664 which corresponds to n-π* transitions (where n is the free doublet on the nitrogen atom of C = N bond and free doublet of S atom on S = C bond). The 610 nm peak is a shoulder, and it corresponds to a vibronic transition 0-1 (level 0 of ground state to level 1 of the excited state). The face-to-face (sandwich-type, H- aggregates) associations of this dye are typically observed in concentrate aqueous solutions. While the 664-nm band is assigned to an isolated molecule (monomer) [55]. The mentioned absorptions peaks were correlated to the dye concentration and were monitored as a direct indicator of the adsorbing effect of added graphite.

The ball-milled graphite samples with the highest SA were tested as agents to remove MB from an aqueous solution and compared with the original sample (Gr0 h). In Fig. 9a, it is noticeable a considerable reduction in MB absorbance signals at initial times (1 and 5 min) due to the effectiveness of graphite (*Gr16hL*) to adsorb the dye. Similar absorption studies were performed with untreated graphite (Gr0 h) (Fig. 9b) and pure milled graphite (Gr16hM) using the same experimental conditions. The adsorption efficiency of the only-milled sample is lower compared to the *Gr16hL* sample. The peak adsorption percentages were 98 and 77% for the Gr16hL and *Gr16hM* samples, respectively, reaching 95% after 30 minutes for the Gr16hL sample. On the other hand, the untreated graphite (Gr0 h) showed no effect on the MB concentration, as can be seen in Fig. 9c. To compare the adsorption performance of the graphitic materials, a plot of adsorbed MB as a function of time is given in Fig. 9d. A fast adsorption level is observed in the Gr16hL sample (near 95%); in comparison, Gr16 h removed only 75% after 30 min. The calculated dye adsorption capacity for the standard concentration (30 mg/L) in the Gr16hL sample after 30 min was found to be around 114 mg/g, which is higher compare to the Gr16 h sample (88.2) and with untreated graphite (0.2). At the beginning of the test, adsorption rate is high, because the high availability of active graphite sites to catch the dye molecules; with further contact time it notices a moderate increase in adsorption level, it can be related with steric impediments faced by ions to occupy available active sites because of the repulsive forces between components (dye and graphite); modifying the chances of MB to be adsorbed.

The removal efficiency reached an optimal after 30 min, showing no further increase after this limit. The image of Fig. 9e shows a visual proof of the dye absorption of MB-Gr solutions reached by the three adsorbents. The solutions adsorbed by Gr16hL shows an almost colorless solution with fully agglomerate graphite particles settled at the bottom of the container (material is easy to separate). The Gr16hM sample produced lower absorption levels compared; it is well dispersed in the solution presenting a fine suspension that cannot settle (even after 24 h of resting); this can be a severe inconvenience related to materials separation from the water after treatment. In contrast, untreated Gr (0 h) is notably inefficient; this is demonstrated by the full blue color of the solution. The increased removal efficiency of Gr16hL sample agrees with its higher surface area and oxygen presence (which induces a negative charge on the surface material), oxygen is generally found in ball-milled samples (see EDS analysis in Fig. 2b), indicating that oxygen and its functional groups play a crucial role in the adsorption process, as was previously reported [56]. The sorption capacity of EG not only depends on the surface area but also on the random pore structure of the material (which has been related with the exfoliation level, pore volume, pore size and its distribution) [4,5,57,58]. Possible adsorption mechanisms of dyes onto graphitic material are related to electrostatic interactions such as Van der Waals forces, delocalized π-orbital: n-π (nitrogen or sulphur donor-acceptor of the dye), π-π (from aromatic rings of the adsorbate) interaction, pore distribution and hydrogen bonding formation on the aqueous solution [56]. In the case of pristine Gr, few available open pores result in weak adsorption due to limited occupancy of active sites for dye molecule.

5. Conclusions

Some exfoliated graphites were prepared following this green and eco-friendly process, avoiding the use of hazardous chemicals, organic solvents and toxic oxidants. The above was eliminated through the use of cheap and common materials processed through a mechanochemical route, representing an alternative method that avoids some disposal problems related to the use of conventional chemicals. There was an evident effect of ball milling time, calcium carbonate addition and the leaching process on the characteristics and performance of prepared samples. The surface area is, in most of the cases, higher or comparable to other aggressive techniques, as can be seen in the summary chart shown in Table 1. The characterization studies confirmed the presence of graphitic structures carbon and graphene in the milled-leached samples. Surface area values increase exponentially with milling time and $CaCO_3$ presence, reaching a maximum of 363 m^2/g in the leached sample, comparing this value with the corresponding SA obtained milling pure graphite (98.6 m^2/g) the difference is evident. Thereby, $CaCO_3$ proved its action as an active agent for Gr exfoliation. EDS mappings confirmed a homogeneous distribution of Gr and the exfoliating agent ($CaCO_3$) after only 1 h of milling; also, the EDS analyses showed the effective acetic acid action removing $CaCO_3$. The evident benefits of the obtained EG in the adsorption of methylene blue (a common pollutant of textile wastewater) were also demonstrated. According to the adsorption testing results, EG represents a useful alternative for dye removal as the adsorption agent reaching efficient levels above 95% after 30 min of testing with MB. Contrary to these results, the untreated graphite sample showed a null adsorption activity against this dye.

CRediT authorship contribution statement

J.M. Mendoza-Duarte: Methodology, Investigation, Validation, Writing - review & editing, Visualization. **F.C. Robles-Hernández:** Conceptualization, Data curation, Visualization. **C.D. Gomez-Esparza:** Conceptualization, Data curation, Visualization. **J.G. Miranda-Hernández:** Software, Validation. **C.G. Garay-Reyes:** Data curation, Investigation, Writing - review & editing. **I. Estrada-Guel:** Validation, Writing - review & editing. **R. Martínez-Sánchez:** Validation, Supervision.

Declaration of Competing Interest

The authors declare that they have no known competing financial interests or personal relationships that could have appeared to influence the work reported in this paper.

Acknowledgments

This research did not receive any specific grant from funding agencies in the public, commercial, or not-for-profit sectors. The authors would like to thank the valuable technical assistance of P. Pizá Ruiz, L. de La Torre Saenz, D. Lardizábal Gutiérrez, and E. Guerrero Lestarjette.

References

[1] E. Sudova, J. Machova, Z. Svobodova, T. Vesely, Negative effects of malachite green and possibilities of its replacement in the treatment of fish eggs and fish: a review, Vet. Med. (Praha). 52 (12) (2007) 527–539, https://doi.org/10.17221/2027-VETMED.

[2] S.H. Sharifi Pajaie, S. Archin, G. Asadpour, Optimization of process parameters by response surface methodology for methylene blue removal using cellulose dusts, Civ. Eng. J. 4 (3) (2018) 620, https://doi.org/10.28991/cej-0309121.

[3] S. Ghorai, A. Sarkar, M. Raoufi, A.B. Panda, H. Schönherr, S. Pal, Enhanced removal of methylene blue and methyl violet dyes from aqueous solution using a nanocomposite of hydrolyzed polyacrylamide grafted xanthan gum and incorporated nanosilica, ACS Appl. Mater. Interfaces 6 (7) (2014) 4766–4777, https://doi.org/

10.1021/am4055657.
[4] E. Kusrini, B. Wicaksono, Y. Yulizar, E.A. Prasetyanto, C. Gunawan, Textile dye removal from aqueous solution using modified graphite waste/lanthanum/chitosan composite, IOP Conf. Ser. Mater. Sci. Eng. 316 (1) (2018), https://doi.org/10.1088/1757-899X/316/1/012029.
[5] N. Sykam, N.D. Jayram, G.M. Rao, Highly efficient removal of toxic organic dyes, chemical solvents and oils by mesoporous exfoliated graphite: synthesis and mechanism, J. Water Process Eng. 25 (2018) 128–137, https://doi.org/10.1016/j.jwpe.2018.05.013 May.
[6] N. Gulnura, K. Kenes, O. Yerdos, M. Zulkhair, R. Di Capua, Preparation of expanded graphite using a thermal method, IOP Conf. Ser. Mater. Sci. Eng. 323 (1) (2018), https://doi.org/10.1088/1757-899X/323/1/012012.
[7] P. Wei, S. Cui, S. Bai, In situ exfoliation of graphite in solid phase for fabrication of graphene/polyamide-6 composites, Compos. Sci. Technol. 153 (2017) 151–159, https://doi.org/10.1016/j.compscitech.2017.10.009.
[8] S.T. Hossain, R. Wang, Electrochemical exfoliation of graphite: effect of temperature and hydrogen peroxide addition, Electrochim. Acta 216 (2016) 253–260, https://doi.org/10.1016/j.electacta.2016.09.022.
[9] F. del Río, M.G. Boado, A. Rama, F. Guitián, A comparative study on different aqueous-phase graphite exfoliation methods for few-layer graphene production and its application in alumina matrix composites, J. Eur. Ceram. Soc. 37 (12) (2017) 3681–3693, https://doi.org/10.1016/j.jeurceramsoc.2017.04.029.
[10] A.R. Kamali, Scalable fabrication of highly conductive 3D graphene by electrochemical exfoliation of graphite in molten NaCl under Ar/H2 atmosphere, J. Ind. Eng. Chem. 52 (2017) 18–27, https://doi.org/10.1016/j.jiec.2017.03.013.
[11] H. Ma, et al., Direct exfoliation of graphite in water with addition of ammonia solution, J. Colloid Interface Sci. 503 (2017) 68–75, https://doi.org/10.1016/j.jcis.2017.04.070.
[12] J. Liu, et al., Improved synthesis of graphene flakes from the multiple electrochemical exfoliation of graphite rod, Nano Energy 2 (no. 3) (2013) 377–386, https://doi.org/10.1016/j.nanoen.2012.11.003.
[13] B. Debelak, K. Lafdi, Use of exfoliated graphite filler to enhance polymer physical properties, Carbon N. Y. 45 (no. 9) (2007) 1727–1734, https://doi.org/10.1016/j.carbon.2007.05.010.
[14] I.M. Afanasov, G. van Tendeloo, A.T. Matveev, Production and structure of exfoliated graphite/coke composites modified by ZrO2 nanoparticles, Xinxing Tan Cailiao/New Carbon Mater. 25 (no. 4) (2010) 255–260, https://doi.org/10.1016/S1872-5805(09)60032-9.
[15] T. Wei, Z. Fan, G. Luo, C. Zheng, D. Xie, A rapid and efficient method to prepare exfoliated graphite by microwave irradiation, Carbon N. Y. 47 (no. 1) (2009) 337–339, https://doi.org/10.1016/j.carbon.2008.10.013.
[16] V.G. Makotchenko, E.D. Grayfer, A.S. Nazarov, S.J. Kim, V.E. Fedorov, The synthesis and properties of highly exfoliated graphites from fluorinated graphite intercalation compounds, Carbon N. Y. 49 (no. 10) (2011) 3233–3241, https://doi.org/10.1016/j.carbon.2011.03.049.
[17] K. Takeuchi, et al., Oil removing properties of exfoliated graphite in actual produced water treatment, *J. Water Process Eng.* 20 (2017) 226–231, https://doi.org/10.1016/j.jwpe.2017.11.009 October.
[18] A.S. Tikhomirov, N.E. Sorokina, O.N. Shornikova, V.A. Morozov, G. Van Tendeloo, V.V. Avdeev, The chemical vapor infiltration of exfoliated graphite to produce carbon/carbon composites, Carbon N. Y. 49 (no. 1) (2011) 147–153, https://doi.org/10.1016/j.carbon.2010.08.054.
[19] X. Van Heerden, H. Badenhorst, The influence of three different intercalation techniques on the microstructure of exfoliated graphite, Carbon N. Y. 88 (2015) 173–184, https://doi.org/10.1016/j.carbon.2015.03.006.
[20] X.J. Yu, J. Wu, Q. Zhao, X.W. Cheng, Preparation and characterization of sulfur-free exfoliated graphite with large exfoliated volume, Mater. Lett. 73 (2012) 11–13, https://doi.org/10.1016/j.matlet.2011.11.078.
[21] H.M.A. Asghar, S.N. Hussain, H. Sattar, N.W. Brown, E.P.L. Roberts, Environmentally friendly preparation of exfoliated graphite, J. Ind. Eng. Chem. 20 (no. 4) (2014) 1936–1941, https://doi.org/10.1016/j.jiec.2013.09.014.
[22] M. Mar, Y. Ahmad, K. Guérin, M. Dubois, N. Batisse, Fluorinated exfoliated graphite as cathode materials for enhanced performances in primary lithium battery, Electrochim. Acta 227 (2017) 18–23, https://doi.org/10.1016/j.electacta.2016.12.137.
[23] M. Dubois, et al., Thermal exfoliation of fluorinated graphite, Carbon N. Y. 77 (2014) 688–704, https://doi.org/10.1016/j.carbon.2014.05.074.
[24] D.A. Siddhanti, et al., The safer and scalable mechanochemical synthesis of edge-chlorinated and fluorinated few-layer graphenes, J. Mater. Sci. 52 (no. 20) (2017) 11977–11987, https://doi.org/10.1007/s10853-017-1237-9.
[25] J. Jagiello, J. Judek, M. Zdrojek, M. Aksienionek, L. Lipinska, Production of graphene composite by direct graphite exfoliation with chitosan, Mater. Chem. Phys. 148 (no. 3) (2014) 507–511, https://doi.org/10.1016/j.matchemphys.2014.09.043.
[26] P. Yu, S.E. Lowe, G.P. Simon, Y.L. Zhong, Electrochemical exfoliation of graphite and production of functional graphene, Curr. Opin. Colloid Interface Sci. 20 (no. 5–6) (2015) 329–338, https://doi.org/10.1016/j.cocis.2015.10.007.
[27] Z.M. Marković, et al., Antibacterial potential of electrochemically exfoliated graphene sheets, J. Colloid Interface Sci. 500 (2017) 30–43, https://doi.org/10.1016/j.jcis.2017.03.110.
[28] A.M. Abdelkader, I.A. Kinloch, Mechanochemical Exfoliation of 2D Crystals in Deep Eutectic Solvents, ACS Sustain. Chem. Eng. 4 (no. 8) (2016) 4465–4472, https://doi.org/10.1021/acssuschemeng.6b01195.
[29] O.Y. Posudievsky, O.A. Khazieieva, V.G. Koshechko, V.D. Pokhodenko, V.V. Cherepanov, High yield of graphene by dispersant-free liquid exfoliation of mechanochemically delaminated graphite, J. Nanoparticle Res. 15 (no. 11) (2013), https://doi.org/10.1007/s11051-013-2046-y.
[30] V. León, A.M. Rodriguez, P. Prieto, M. Prato, E. Vázquez, Exfoliation of graphite with trriazine derivatives under ball-milling conditions: Preparation of few-layer graphene via selective noncovalent interactions, ACS Nano 8 (no. 1) (2014) 563–571, https://doi.org/10.1021/nn405148t.
[31] A. Amiri, et al., Facile, environmentally friendly, cost effective and scalable production of few-layered graphene, Chem. Eng. J. 326 (2017) 1105–1115, https://doi.org/10.1016/j.cej.2017.06.046.
[32] I.Y. Jeon, et al., Large-scale production of edge-selectively functionalized graphene nanoplatelets via ball milling and their use as metal-free electrocatalysts for oxygen reduction reaction, J. Am. Chem. Soc. 135 (no. 4) (2013) 1386–1393, https://doi.org/10.1021/ja3091643.
[33] Q. Zhao, X. Cheng, J. Wu, X. Yu, Sulfur-free exfoliated graphite with large exfoliated volume: Preparation, characterization and its adsorption performance, J. Ind. Eng. Chem. 20 (no. 6) (2014) 4028–4032, https://doi.org/10.1016/j.jiec.2014.01.002.
[34] F. Jiang, Y. Yu, Y. Wang, A. Feng, L. Song, A novel synthesis route of graphene via microwave assisted intercalation-exfoliation of graphite, Mater. Lett. 200 (2017) 39–42, https://doi.org/10.1016/j.matlet.2017.04.048.
[35] X.H. Wei, L. Liu, J.X. Zhang, J.L. Shi, Q.G. Guo, HClO4-graphite intercalation compound and its thermally exfoliated graphite, Mater. Lett. 63 (no. 18–19) (2009) 1618–1620, https://doi.org/10.1016/j.matlet.2009.04.030.
[36] J.M. Mendoza-Duarte, R. Martinez-Sanchez, I. Estrada-Guel, Effect of high-energy ball milling on the microstructure of natural graphite, Microsc. Microanal. 19 (S2) (2013) 1598–1599, https://doi.org/10.1017/s1431927613009987.
[37] R.P. Campos, A.C. Cuevas, R.E. Muñoz, Materials characterization, Mater. Charact. (2015) 1–223, https://doi.org/10.1007/978-3-319-15204-2.
[38] J. Zhou, et al., A gas bubble exfoliation method to prepare g-C3N4 nanosheets with enhanced photocatalytic activities, J. Photochem. Photobiol. A 372 (2019) 147–155, https://doi.org/10.1016/j.jphotochem.2018.11.040 November 2018.
[39] I. Papailias, et al., Chemical vs thermal exfoliation of g-C3N4 for NOx removal under visible light irradiation, Appl. Catal. B 239 (July) (2018) 16–26, https://doi.org/10.1016/j.apcatb.2018.07.078.
[40] S. You, S.M. Luzan, T. Szabó, A.V. Talyzin, Effect of synthesis method on solvation and exfoliation of graphite oxide, Carbon N. Y. 52 (2013) 171–180, https://doi.org/10.1016/j.carbon.2012.09.018.
[41] F. Jiang, Y. Yu, A. Feng, L. Song, Effects of ammonia on graphene preparation via microwave assisted intercalation exfoliation method, Ceram. Int. 44 (no. 11) (2018) 12763–12766, https://doi.org/10.1016/j.ceramint.2018.04.081.
[42] B.D. Ossonon, D. Bélanger, Functionalization of graphene sheets by the diazonium chemistry during electrochemical exfoliation of graphite, Carbon N. Y. 111 (2017) 83–93, https://doi.org/10.1016/j.carbon.2016.09.063.
[43] H.G. Kang, et al., Scalable exfoliation and activation of graphite into porous graphene using microwaves for high–performance supercapacitors, J. Alloys Compd. 770 (2019) 458–465, https://doi.org/10.1016/j.jallcom.2018.08.042.
[44] P. Krawczyk, B. Gurzęda, A. Bachar, Thermal exfoliation of electrochemically obtained graphitic materials, Appl. Surf. Sci. 481 (2019) 466–472, https://doi.org/10.1016/j.apsusc.2019.03.154 no. November 2018.
[45] N.E. Sorokina, A.V. Redchitz, S.G. Ionov, V.V. Avdeev, Different exfoliated graphite as a base of sealing materials, J. Phys. Chem. Solids 67 (no. 5–6) (2006) 1202–1204, https://doi.org/10.1016/j.jpcs.2006.01.048.
[46] K. Takeuchi, et al., Oil sorption by exfoliated graphite from dilute oil-water emulsion for practical applications in produced water treatments, J. Water Process Eng. 8 (2015) 91–98, https://doi.org/10.1016/j.jwpe.2015.09.002.
[47] S.H. Song, H.K. Jeong, Y.G. Kang, Preparation and characterization of exfoliated graphite and its styrene butadiene rubber nanocomposites, J. Ind. Eng. Chem. 16 (no. 6) (2010) 1059–1065, https://doi.org/10.1016/j.jiec.2010.07.004.
[48] S.P. Gumfekar, Graphene-Based Materials for Clean Energy Applications, Elsevier Inc., 2018.
[49] S. Sharma, D. Susan, N.C. Kothiyal, R. Kaur, Graphene oxide prepared from mechanically milled graphite: Effect on strength of novel fly-ash based cementitious matrix, Constr. Build. Mater. 177 (2018) 10–22, https://doi.org/10.1016/j.conbuildmat.2018.05.051.
[50] C.S. Wang, G.T. Wu, W.Z. Li, Lithium insertion in ball-milled graphite, J. Power Sources 76 (no. 1) (1998) 1–10, https://doi.org/10.1016/S0378-7753(98)00114-1.
[51] D.H. Gharib, S. Gietman, F. Malherbe, S.E. Moulton, High yield, solid exfoliation and liquid dispersion of graphite driven by a donor-acceptor interaction, Carbon N. Y. 123 (2017) 695–707, https://doi.org/10.1016/j.carbon.2017.08.025.
[52] H.A. Calderon, I. Estrada-Guel, F. Alvarez-Ramírez, V.G. Hadjiev, F.C. Robles Hernandez, Morphed graphene nanostructures: Experimental evidence for existence, Carbon N. Y. 102 (2016) 288–296, https://doi.org/10.1016/j.carbon.2016.02.056.
[53] H.A. Calderon, A. Okonkwo, I. Estrada-Guel, V.G. Hadjiev, F. Alvarez-Ramírez, F.C. Robles Hernández, HRTEM low dose: the unfold of the morphed graphene, from amorphous carbon to morphed graphenes, Adv. Struct. Chem. Imaging 2 (no. 1) (2016), https://doi.org/10.1186/s40679-016-0024-z.
[54] K. Bai, J.C. Fan, P.H. Shi, Y.L. Min, Q.J. Xu, Directly ball milling red phosphorus and expended graphite for oxygen evolution reaction, J. Power Sources 456 (no. January) (2020) 228003, https://doi.org/10.1016/j.jpowsour.2020.228003.
[55] D. Heger, J. Jirkovský, P. Klán, Aggregation of methylene blue in frozen aqueous solutions studied by absorption spectroscopy, J. Phys. Chem. A 109 (no. 30) (2005) 6702–6709, https://doi.org/10.1021/jp050439j.
[56] J.A. Mattson, H.B. Mark, M.D. Malbin, W.J. Weber, J.C. Crittenden, Surface chemistry of active carbon: specific adsorption of phenols, J. Colloid Interface Sci. 31 (1) (1969) 116–130, https://doi.org/10.1016/0021-9797(69)90089-7.
[57] M. Toyoda, M. Inagaki, Heavy oil sorption using exfoliated graphite new application of exfoliated graphite to protect heavy oil pollution, Carbon N. Y. 38 (no. 2) (2000) 199–210, https://doi.org/10.1016/S0008-6223(99)00174-8.
[58] M. Toyoda, M. Inagaki, Sorption and recovery of heavy oils by using exfoliated graphite, Spill Sci. Technol. Bull. 8 (no. 5–6) (2003) 467–474, https://doi.org/10.1016/S1353-2561(03)00131-2.